

Elemental behavior during chlorite alteration: New insights from a combined EMPA and LA-ICPMS study in porphyry Cu systems

Bing Xiao, Huayong Chen*

Key Laboratory of Mineralogy and Metallogeny, Guangzhou Institute of Geochemistry, Chinese Academy of Sciences, Guangzhou 510640, China

ARTICLE INFO

Editor: Dong Hailiang

Keywords:

Chlorite
Element behavior
Mineral chemistry
Precursor minerals
Porphyry deposits

ABSTRACT

Chlorite is a common alteration product of fluid-rock interaction in hydrothermal deposits, and its compositional variations provides useful information about the physicochemical conditions of formation, but element behavior during the chloritization process is still not well understood. Chlorite from two large porphyry Cu deposits, Atlas (Philippines) and Xiaokelehe (NE China) have been chosen to evaluate the geochemical variations with a focus on mass transfer during alteration of precursor minerals.

Conversion of two biotite to one chlorite is the main mechanism for the chloritization of biotite. Iron, Mg, Al, and Ni are mostly retained in chlorite, whereas Co, Ga, Mn, and Zn are commonly transferred to chlorite from the hydrothermal fluid, and Sc, Sr, Si, V, Li, K, Nb, Ba, Rb, Ti, Cl, Na, Sn, and Cu from the biotite mostly do not enter chlorite during chloritization. Chlorite alteration of hornblende formed probably through the processes of dissolution-precipitation. Iron are mostly retained in the chlorite, whereas Li, Cu, Ni, Zn, Co, Al, and Ga in the chlorite are at least in part derived from hydrothermal fluid, and Mg, Mn, V, Si, Ca, Zr, Nb, Sn, Cl, REE, Y, Na, Ti, Sr, K, Sc and Ba originally in the hornblende mostly enter hydrothermal fluid, titanite or epidote, rather than chlorite during chloritization. The MgO, FeO_T, MnO, Zn, Li, Sc, V, Co and Ni concentrations, and FeO_T/MgO ratio of chlorite are strongly influenced by those of the precursor minerals. Moreover, although formed in the same porphyry system, the MnO, Zn, Li and Cu concentrations and FeO_T/MgO ratios of chlorite formed from biotite and hornblende are markedly different.

Given that Fe/Mg ratios of chlorite are controlled by the precursor minerals in wall rock, the Fe/(Fe + Mg) correction on the well-established chlorite thermometers during hydrothermal alteration may need to be re-considered. Aluminum, Ga, and Ti in chlorite are not controlled by precursor minerals, but by formation temperature of chlorite, so we can use these elements of chlorite to map out the thermal structure of porphyry system which is related to individual mineralized porphyry intrusion, which can help to identify the centers of hydrothermal systems.

1. Introduction

Chlorite is one of the most widely developed alteration minerals in hydrothermal systems forming in diverse geological settings associated with a variety of ore deposits including Cu, Au and U deposits (Sillitoe, 2010; Zhong et al., 2012; Dora and Randive, 2015; Brzowski et al., 2018). The variable chemical compositions of chlorite record information about the physicochemical conditions of their formation, and are therefore highly useful in characterizing the hydrothermal alteration process and estimating the temperature of ore formation (Cathelineau, 1988; Yavuz et al., 2015). A recent study at Batu Hijau (Indonesia) has shown that major- and trace-elements of chlorite in porphyry systems can provide lateral and vertical elemental variation trends (Wilkinson et al., 2015), and can be used as a mineral

geochemical vectoring tool in the exploration for porphyry deposits in a given district (Hart et al., 2016; Brzowski et al., 2018; Xiao et al., 2018). Nevertheless, our understanding of element behavior and especially the mass transfer during chloritization is still inadequate, which limits its application both as a geothermometer and for geochemical vectoring towards hydrothermal deposits.

Chlorite group minerals are hydrous phyllosilicates in which adjacent 2:1 talc layers are linked by an octahedral brucite sheet (Krivovichev et al., 2004), and mainly from through replacement of ferromagnesian minerals (e.g., biotite and hornblende) during fluid-rock interaction (Walker, 1993). Chlorite has a wide range of stoichiometric compositions, which may be related to the compositions of the minerals they have replaced, the composition of the hydrothermal fluids from which they precipitated, and their formation temperatures

* Corresponding author.

E-mail address: huayongchen@gig.ac.cn (H. Chen).

<https://doi.org/10.1016/j.chemgeo.2020.119604>

Received 19 December 2019; Received in revised form 28 March 2020; Accepted 30 March 2020

Available online 03 April 2020

0009-2541/ © 2020 Elsevier B.V. All rights reserved.

(from 40 °C to 600 °C; Beaufort et al., 2015). Although previous research has shown that Fe/Mg ratios of chlorite are positively correlated with those of wall rock (Kranidiotis and MacLean, 1987; Shikazono and Kawahata, 1987), the genetic mechanism is not yet well understood. In this study, we present combined electron probe microanalysis (EPMA) and laser ablation inductively-coupled plasma mass spectrometry (LA-ICP-MS) data for chlorite, biotite, and hornblende from the two representative porphyry-type deposits. We firstly provided a detailed investigation of element mass transferring during biotite and hornblende chloritization, which is one of the most important hydrothermal alteration processes. Furthermore, we evaluated the effect of precursor minerals on chlorite, which is critical for the current application of chlorite on both ore genesis and mineral exploration targeting.

2. Geological setting and sampling

2.1. Deposit geology

The newly discovered Mesozoic Xiaokelehe porphyry Cu–Mo deposit (250 Mt ore @ 0.2 wt% Cu and @ 0.03–0.8 wt% Mo; Shang, 2017) is situated in the northeastern part of the Great Hingan Range metallogenic belt, NE China (Fig. 1), in the eastern sector of the Central Asia Orogenic Belt. Copper–Mo mineralization dominantly occurs in the granodiorite porphyry and sodic-calcic, potassic, chlorite, and phyllic alteration have been identified, with chlorite as the most abundant alteration mineral (Shang, 2017; Feng et al., 2019). The Xiaokelehe granodiorite porphyry is light gray in color, and displays porphyritic-like textures and is mainly composed of plagioclase (~30 vol%), quartz (~20 vol%), biotite (~10 vol%), and K-feldspar (~10 vol%), with minor hornblende as phenocrysts (Fig. 2a). Plagioclase and K-feldspar phenocrysts in the Xiaokelehe granodiorite porphyry occur as subhedral to euhedral crystals, that have

been partially replaced by illite. Biotite has been partially or wholly altered to chlorite + titanite (\pm rutile; Fig. 2b).

The giant Atlas porphyry Cu–Au deposit (1420 Mt ore @ 0.45 wt% Cu and 0.24 g/t Au), situated approximately 30 km west of Cebu City on Cebu Island, Philippines (Fig. 1), is the oldest porphyry deposit in the Philippines with a whole-rock Rb–Sr age of 108 ± 1 Ma (Singer et al., 2008; Zhang et al., 2019). Hydrothermal alteration and mineralization at the Atlas Cu–Au deposit have been divided into potassic, propylitic, and phyllic zones (Sillitoe and Gappe, 1984; Zhang et al., 2019). The Atlas quartz diorite porphyry is coarse-grained, gray in color, and contains ~75 vol% phenocrysts (~50 vol% plagioclase, ~25 vol% amphibole and minor biotite) in a microcrystalline quartz, K-feldspar and plagioclase groundmass (Fig. 2c). Plagioclase phenocrysts occur as subhedral to euhedral crystals, which are partially replaced by illite. Biotite phenocrysts occur as euhedral crystals that have been partially or wholly altered to chlorite + titanite (Fig. 2d). Hornblende phenocrysts also occur as euhedral crystals that have been partially altered to chlorite + titanite \pm epidote (Fig. 2e).

2.2. Sampling

In this study, 35 samples from 7 drill cores at Xiaokelehe and 30 samples from 4 drill cores at Atlas were collected for petrographic study. Forty-five polished thin sections were prepared and studied using transmitted and reflected light microscopy, and representative samples were then analyzed with EMPA to aid mineral identification and determine compositions. Samples containing chlorite were all selected from major alteration zones of the porphyry deposits. They include chlorite alteration of: 1) biotite in the Xiaokelehe granodiorite (Fig. 2b); 2) biotite in the Atlas quartz diorite (Fig. 2d); 3) hornblende in the Atlas quartz diorite (Fig. 2e).

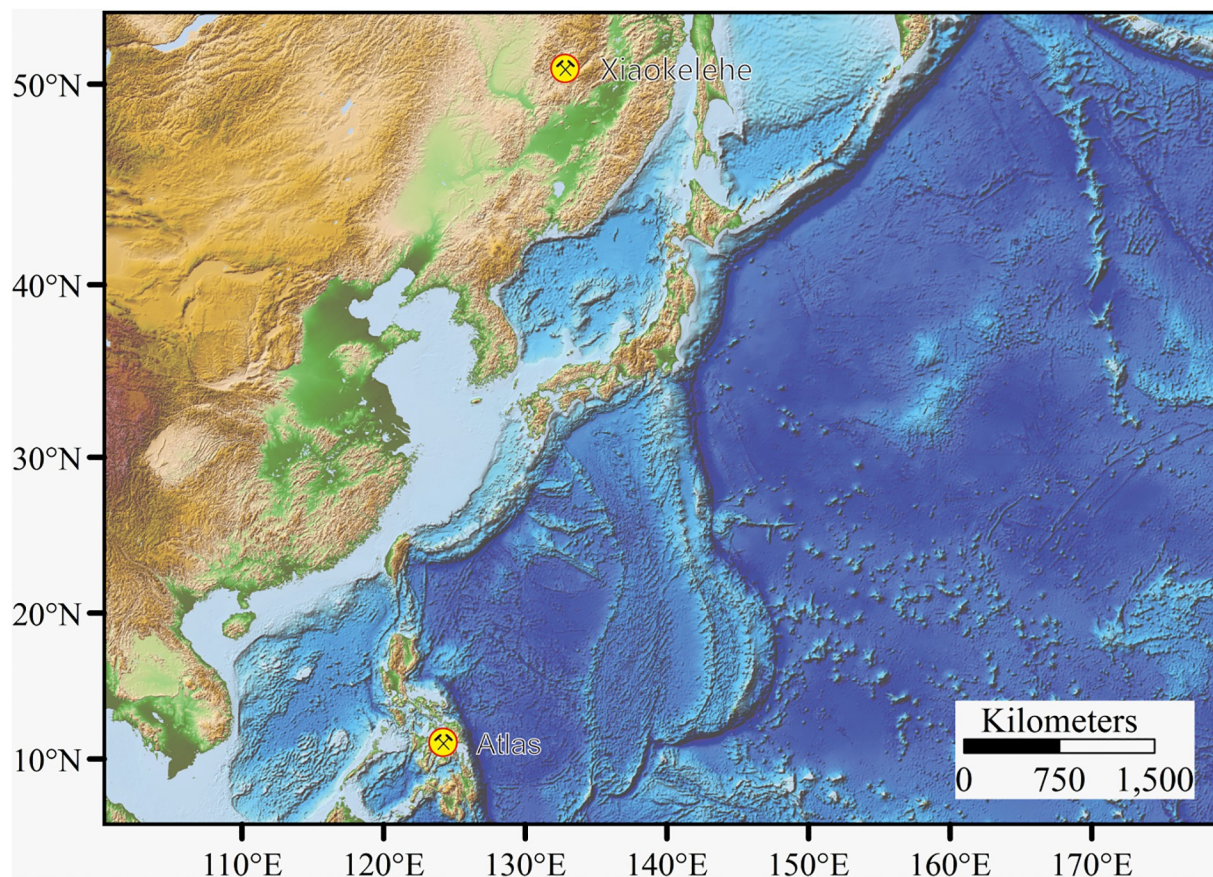


Fig. 1. Location of the Atlas and Xiaokelehe porphyry Cu deposits in this study.

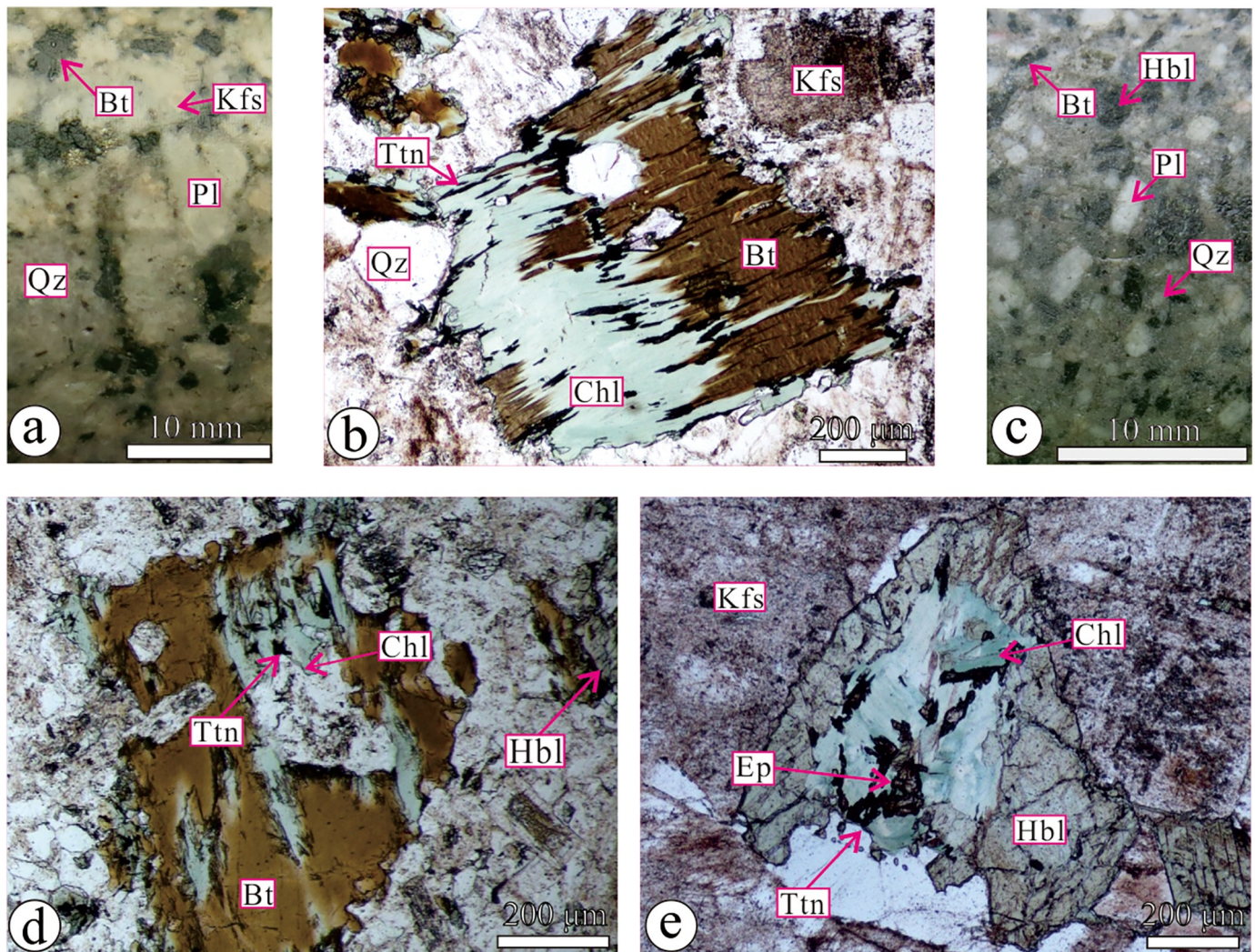


Fig. 2. Hand specimen photographs and microphotographs showing representative mineral assemblages, textural features and chloritization of the Xiaokelehe granodiorite porphyry and Atlas quartz diorite porphyry. (a) The Xiaokelehe granodiorite porphyry contains plagioclase, quartz, biotite, and K-feldspar phenocrysts generally < 0.5 cm (51°40'53"N, 124°32'5.3"E, Elevation = -50 m); (b) K-feldspar, biotite and quartz phenocrysts of the Xiaokelehe granodiorite porphyry in a fine-grained groundmass of K-feldspar and quartz. Biotite is partially replaced by chlorite. (c) The Atlas quartz diorite porphyry contains plagioclase, biotite, and amphibole phenocrysts generally < 0.4 cm (10°20'0.25"N, 123°43'46.58"E, Elevation = 91 m); (d) and (e) Hornblende and biotite phenocrysts of the Atlas quartz diorite porphyry in a fine-grained groundmass of K-feldspar, quartz, and plagioclase. Biotite and amphibole is replaced by chlorite. Mineral abbreviations: Bt, biotite; Chl, chlorite; Hbl, hornblende; Kfs, K-feldspar; Pl, plagioclase; Qz, quartz.

3. Analytical procedures

Back-scattered electron (BSE) and major element analyses of chlorite, biotite, and hornblende were conducted using a Cameca SX100 electron microprobe at the Guangzhou Institute of Geochemistry (GIG), Chinese Academy of Sciences (CAS) with a JEOL JXA-8230 Superprobe. EPMA results are listed in Electronic Appendix I. The following conditions were used for measurements of all standards and samples: 15 kV accelerating voltage, 20 nA beam current, 1 μm beam diameter, 10 s counting time. To correct for the matrix effects during EPMA, a matrix correction, the so called ZAF correction, is applied to transform the relative peak intensities into the elemental weight composition (Bernard et al., 1986). Relative precisions are < 2% for major elements and < 5% for minor elements.

Trace elements of chlorite were determined using a NWR Laser Ablation system coupled with an iCAP RQ ICP-MS at the Guangzhou Tuoyan Analytical Technology Co., Ltd., Guangzhou, China. Fifty-one elements (Li⁷, B¹¹, Na²³, Mg²⁵, Al²⁷, Si²⁹, Fe⁵⁷, K³⁹, Ca⁴³, Sc⁴⁵, Ti⁴⁷, V⁵¹, Mn⁵⁵, Co⁵⁹, Ni⁶⁰, Cu⁶⁵, Zn⁶⁶, Ga⁷¹, As⁷⁵, Rb⁸⁵, Sr⁸⁸, Y⁸⁹, Zr⁹¹, Nb⁹³, Mo⁹⁷, Cd¹¹¹, Sn¹¹⁸, Sb¹²¹, Cs¹³³, Ba¹³⁵, La¹³⁹, Ce¹⁴⁰, Pr¹⁴¹, Nd¹⁴⁶,

Sm¹⁴⁷, Eu¹⁵¹, Gd¹⁵⁷, Tb¹⁵⁹, Dy¹⁶¹, Ho¹⁶⁵, Er¹⁶⁶, Tm¹⁶⁹, Yb¹⁷², Lu¹⁷⁵, Hf¹⁷⁸, Ta¹⁸¹, W¹⁸², Au¹⁹⁷, Pb²⁰⁸, Th²³², and U²³⁸) were analyzed in chlorite, biotite, and hornblende by LA-ICP-MS. The ablation was carried out across the surface of chlorite, biotite, and hornblende grains to obtain relatively homogeneous composition and avoid visible mineral inclusions. A "wire" signal smoothing device is included in this laser ablation system. These minerals were ablated using spot sizes ranging from 30 μm using a pulse energy density of ca. 8.0 J/cm² and pulse repetition rate of 8 Hz. Laser ablation was conducted in pure He gas flowing at a rate of 0.68 L/min. Immediately after the ablation point in the cell, the He carrier gas was mixed with Ar (0.68 L/min) to improve the aerosol transport efficiency. Operating conditions included: RF power of 1250 W, Detector mode of STD, oxide and double-charged ion production rates of < 0.025% and < 0.02%. Dwell times on each mass varied from 5 to 50 ms, depending on the count rates. The concentrations of fifty-one elements were determined during each analysis, which consisted of an initial 50 s to measure the gas blank followed by up to 40 s of sample ablation, for a total analysis time of 90 s. Analyses were calibrated using three external standards (BHVO-2G, NIST-612 and NIST-610). The samples were analyzed by LA-ICP-MS, also by EPMA.

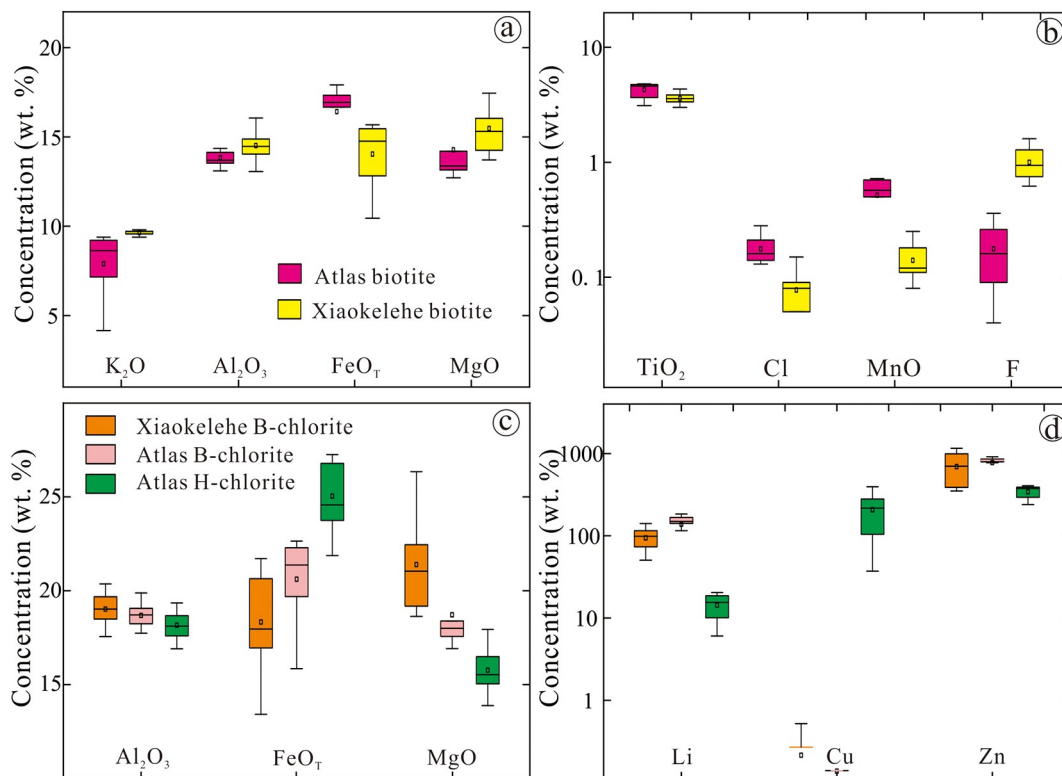


Fig. 3. Comparison of Atlas and Xiaokelehe biotite (a and b), and Xiaokelehe and Atlas B-chlorite, and Atlas H-chlorite (c and d).

Every LA-ICP-MS data has been corrected by EPMA data, using Al₂O₃ as internal standardization for chlorite and biotite, and CaO for hornblende, respectively. An Excel-based software ilolite was used to perform off-line selection and integration of background and analyzed signals, time-drift correction and quantitative calibration for trace element analysis. Detection limits are 0.71 to 26 ppm for Li⁷, 4.70 to 150 ppm for Na²³, 1000 to 11,000 ppm for Mg²⁵, 1800 to 18,000 ppm for Si²⁹, 3.9 to 10,000 ppm for K³⁹, 340 to 2200 ppm for Ca⁴³, 0.49 to 11 ppm for Sc⁴⁵, 5.20 to 3200 ppm for Ti⁴⁷, 5.00 to 110 ppm for V⁵¹, 25 to 880 ppm for Mn⁵⁵, 1.10 to 12 ppm for Co⁵⁹, 2.30 to 42 ppm for Ni⁶⁰, 0.01 to 40 ppm for Cu⁶⁵, 6.60 to 77 ppm for Zn⁶⁶, 1.60 to 16 ppm for Ga⁷¹, 0.1 to 64 ppm for Rb⁸⁵, 0.16 to 8.9 ppm for Sr⁸⁸, 0.03 to 2.2 ppm for Y⁸⁹, 0.01 to 3.1 ppm for Zr⁹¹, 0.01 to 7 ppm for Nb⁹³, 0.22 to 2.5 ppm for Sn¹¹⁸, 0.18 to 1.7 ppm for Sb¹²¹, 0.03 to 21 ppm for Cs¹³³, 0.21 to 720 ppm for Ba¹³⁵, 0.01 to 1 ppm for Ta¹⁸¹, 0.01 to 2.8 ppm for Pb²⁰⁸, 0.01 to 1 ppm for Th²³², and 0.01 to 1 ppm for U²³⁸. LA-ICP-MS results are listed in Electronic Appendix II.

In this study, the contents of FeO_T, MgO, K₂O, Na₂O, Al₂O₃, SiO₂, TiO₂, and MnO of chlorite, biotite, and hornblende were analyzed by both EMPA and LA-ICP-MS. EMPA and LA-ICP-MS are more suitable for analyzing major and trace elements, respectively. Hence, the contents of SiO₂, Al₂O₃, FeO and MgO of chlorite, K₂O, SiO₂, Al₂O₃, FeO and MgO of biotite, CaO, SiO₂, Al₂O₃, FeO and MgO of hornblende, were from EMPA, and those of other elements were from LA-ICP-MS.

4. Mineral chemistry

4.1. Major element data for hornblende, biotite and chlorite

Hornblende, biotite, and chlorite EMPA results are listed in Appendix I. Compared with Xiaokelehe biotite, Atlas biotite contains higher FeO_T, TiO₂, Cl, and MnO, and lower MgO, K₂O, Al₂O₃, and F (Fig. 3a and b). The crystallochemical formula of Xiaokelehe and Atlas biotite can be written as: K_{0.82-1.80}Mg_{2.79-4.30}Fe_{1.53-2.29}Al_{2.33-2.76}Si_{5.47-5.70}Ti_{0.36-0.54}Mn_{0.01-0.09}O₂₂(OH)₄ and K_{1.74-1.85}Mg_{3.00-4.07}Fe_{1.25-1.93}Al_{2.28-2.77}Si_{5.47-5.77}Ti_{0.33-0.48}

Mn_{0.01-0.03}O₂₂(OH)₄, respectively. Two samples have obviously lower FeO_T, MnO, and higher MgO than other samples of Atlas biotite, which may be due to biotite of these samples being hydrothermal, rather than magmatic biotite (Appendix I). The contents of CaO for the Xiaokelehe and Atlas biotite are close to, or below, the detection limits of EMPA. The crystallochemical formula of the Atlas hornblende can be written as: (K_{0.05-0.13}Na_{0.11-0.30}Ca_{1.69-1.90}Mg_{2.49-2.99}Fe_{1.95-2.36}Al_{0.68-1.25}Si_{6.68-7.29}Ti_{0.06-0.18}Mn_{0.03-0.07}O₂₂(OH)₂). From chlorite of the Xiaokelehe biotite chloritization (Xiaokelehe B-chlorite, Mg_{2.86-3.87}Al_{2.04-2.49}Fe_{1.11-1.87}Mn_{0.01-0.03}Si_{2.76-2.96}O₁₀(OH)₈), chlorite of the Atlas biotite chloritization (Atlas B-chlorite, Mg_{2.65-3.41}Al_{2.20-2.41}Fe_{1.33-1.99}Mn_{0.01-0.13}Si_{2.84-2.97}O₁₀(OH)₈), to chlorite of the Atlas hornblende chloritization (Atlas H-chlorite, Mg_{2.25-2.78}Al_{2.08-2.38}Fe_{1.90-2.47}Mn_{0.03-0.04}Si_{2.82-3.09}O₁₀(OH)₈), MgO contents gradually increase, while FeO_T contents gradually decrease (Fig. 3c). The CaO, Na₂O, and K₂O contents of Xiaokelehe B-chlorite, Atlas B-chlorite and H-chlorite, all are close to, or below, the detection limits of EMPA. In the R²⁺ vs. Si (a.p.f.u) diagram, based on the chemical compositions and mineral crystal structure, all three types of chlorite are plotted in the tri-trioctahedral field and close to the end-member of clinocllore and chamosite (Fig. 4; Wiewióra and Weiss, 1990). In this study, correlation coefficients were calculated to determine the relationship between chemical components of chlorite and precursor minerals, and the important relationships are illustrated in Figs. 5–7 and Appendix III. The FeO_T, MgO and MnO contents of chlorite are strongly positively correlated with that of biotite in Xiaokelehe and Atlas (Fig. 5), and the FeO_T and MgO contents show weakly positively correlated with that of Atlas hornblende (Fig. 6).

4.2. Trace element data for hornblende, biotite and chlorite

Trace element concentrations of selected elements for hornblende, biotite, and chlorite are given in Appendix II. Xiaokelehe and Atlas biotite have similar trace elements pattern: high contents of V and Rb (~200 to 1000 ppm), moderate contents of Li, Sc, Co, Ni, Ga, Ba (~10 ppm to 100 ppm), and low contents of Sr, Nb, Sn, Pb (~1 ppm to

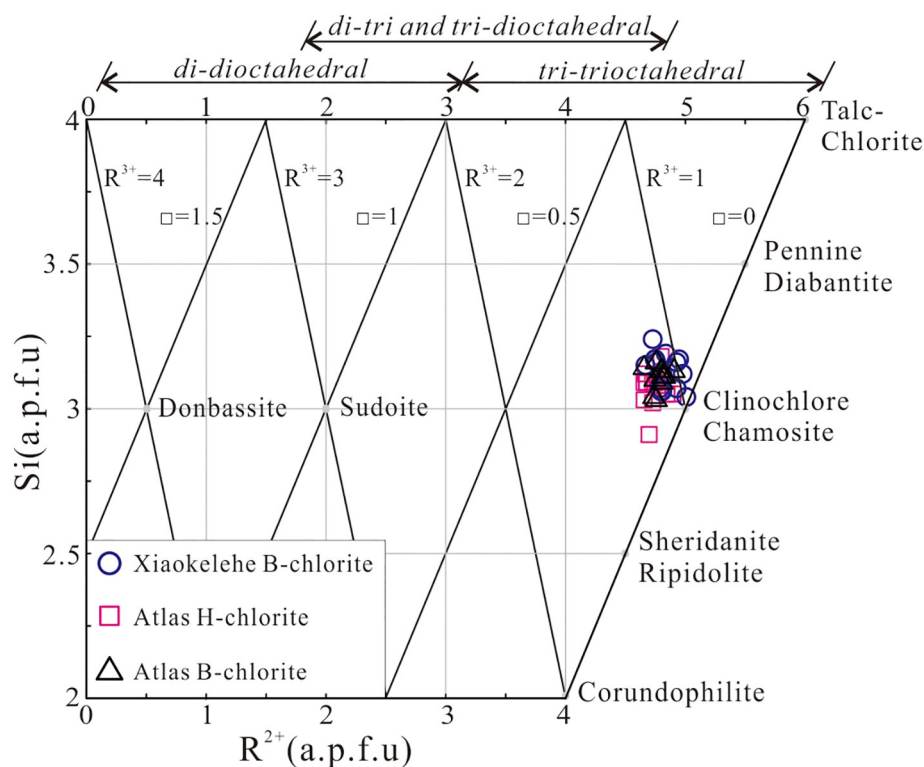


Fig. 4. Chlorite classification of the Atlas and Xiaokelehe porphyry Cu deposits (after Wiewióra and Weiss, 1990).

10 ppm), and concentrations of other elements, e.g., B, Ca, Cu, As, Rb, Y, Zr, Mo, Cd, Sn, Sb, Cs, REE, Hf, Ta, W, Au, Th, U are either close to or below the detection limits of LA-ICP-MS. The Atlas hornblende analyses yielded high contents of V, Zn, and REE (~100 ppm to 600 ppm), moderate contents of Sc, Co, Ni, Y, and Zr, (10–200 ppm) and low contents of Cu, Ga, Sr, Nb, Sn, Hf, Ta, Pb (~1–50 ppm), whereas concentrations of other elements, e.g., Li, B, As, Rb, Mo, Cd, Sb, Cs, W, Au, Th, U, are either close to or below the detection limits of LA-ICP-MS. In general, Zn and V are the most abundant trace elements (ranging from 100 ppm to 1500 ppm) in Xiaokelehe B-chlorite, Atlas B-chlorite and H-chlorite. These three types of chlorite all show wide variations in K and Ti (~10 ppm to 1000 ppm), moderate contents of Sc, Co, Ni and Ga (most ranging from ~10 ppm to 100 ppm), and low contents of Sr and Ba (~1 ppm to 10 ppm), whereas concentrations of other elements, e.g., B, Ca, Na, As, Rb, Y, Zr, Nb, Mo, Cd, Sn, Sb, Cs, REE, Ta, W, Au, Pb, Th, U, are either close to or below the detection limits of LA-ICP-MS. Compared with Atlas H-chlorite, Xiaokelehe and Atlas B-chlorite have higher Li and Zn contents (Fig. 3d). Moreover, Xiaokelehe and Atlas B-chlorite both contain no Cu, while the Cu contents of Atlas H-chlorite range from 36.1 ppm to 708 ppm (Fig. 3d). The Co, Ni, Zn, Sc, V, and Li contents of chlorite are strongly positively correlated with that of biotite in Xiaokelehe and Atlas (Fig. 5), and the Ni content of chlorite is weakly correlated with that of biotite in Xiaokelehe and Atlas (Fig. 6).

5. Discussion

5.1. Elemental behaviors in chloritization process

Aluminum, Mn, and Ti are generally considered immobile or least-mobile elements during fluid-rock interaction processes, and consequently previous studies have investigated element transfer during biotite chloritization under the assumption that Al, Mn, or Ti should remain constant during biotite alteration (Parry and Downey, 1982; Yuguchi et al., 2015; Wang et al., 2018). In this study, we compared the measured contents of elements in Xiaokelehe and Atlas B-chlorite, and Atlas H-chlorite with ideal chlorite compositions, in order to investigate

element transfer between chlorite and biotite/hornblende during alteration. The biotite chloritization reaction can be shown as: Biotite + hydrothermal fluid → chlorite + titanite. The molecular weight of chlorite (M_{Chl}) and biotite (M_{Bt}) could be obtained based on the EPMA data and calculations of structural formulas. If an element (such as Fe) in biotite all enter chlorite during chloritization, we can get the equation: $M_{\text{Chl}} \times C_{\text{Fe in Chl}} = M_{\text{Bt}} \times M_{\text{Fe in Bt}}$ where $M_{\text{Fe in Bt}}$ is the measured content of Fe in biotite, and $C_{\text{Fe in Chl}}$ can be calculated based on the above equation. Then, if the $C_{\text{Fe in Chl}}$ is lower than $M_{\text{Fe in Chl}}$ (the measured content of Fe in chlorite), it suggests that part of Fe in chlorite is from hydrothermal fluid, and if the $C_{\text{Fe in Chl}}$ is higher than $M_{\text{Fe in Chl}}$, indicating part of Fe in biotite do not enter chlorite during biotite chloritization. By comparing the $C_{\text{Fe in Chl}}$ and $M_{\text{Fe in Chl}}$, we could also get the proportions of elements in biotite entering chlorite or hydrothermal fluid and coexisting minerals. Analogously, we can get the calculated values of elements in chlorite from hornblende chloritization, and the results are shown in Tables 1 and 2.

By comparing the calculated and analytical values of elements in chlorite, it can be seen that the FeO_T (avg. 92%), Ni (avg. 92%), Al_2O_3 (avg. 95%), and MgO (avg. 97%) in Xiaokelehe and Atlas biotite are mostly retained in the chlorite; part of Co (avg. 18%), Ga (avg. 23%), MnO (avg. 29%), and Zn (avg. 52%) in Xiaokelehe and Atlas B-chlorite were derived from hydrothermal fluids; and Sc (avg. 73%), Sr (avg. 58%), SiO_2 (avg. 47%), V (avg. 37%), and Li (avg. 27%) in Xiaokelehe and Atlas biotite entered hydrothermal fluids or titanite, rather than chlorite (Fig. 5). In addition, the K, Nb, Ba, Rb, Ti, Cl, Na, Sn, and Cu contents of Xiaokelehe and Atlas B-chlorite are orders of magnitude lower than that of Xiaokelehe and Atlas biotite (Appendixes I and II), suggesting that the process of biotite chloritization results in K (almost 100%), Nb (almost 100%), Ba (almost 100%), Rb (almost 100%), Ti (avg. 98%), Cl (avg. 96%), Na (avg. 93%), Sn (avg. 90%), and Cu (avg. 82%) in biotite entering the hydrothermal fluid, titanite, or rutile rather than chlorite. Elements behavior in the biotite chloritization processes could be controlled by solubility of elements in biotite and chlorite. Titanite could accommodate Ti, Nb, and Sn, and rutile could accommodate Ti and Nb (Fu et al., 2018; Foley et al., 2000). These results

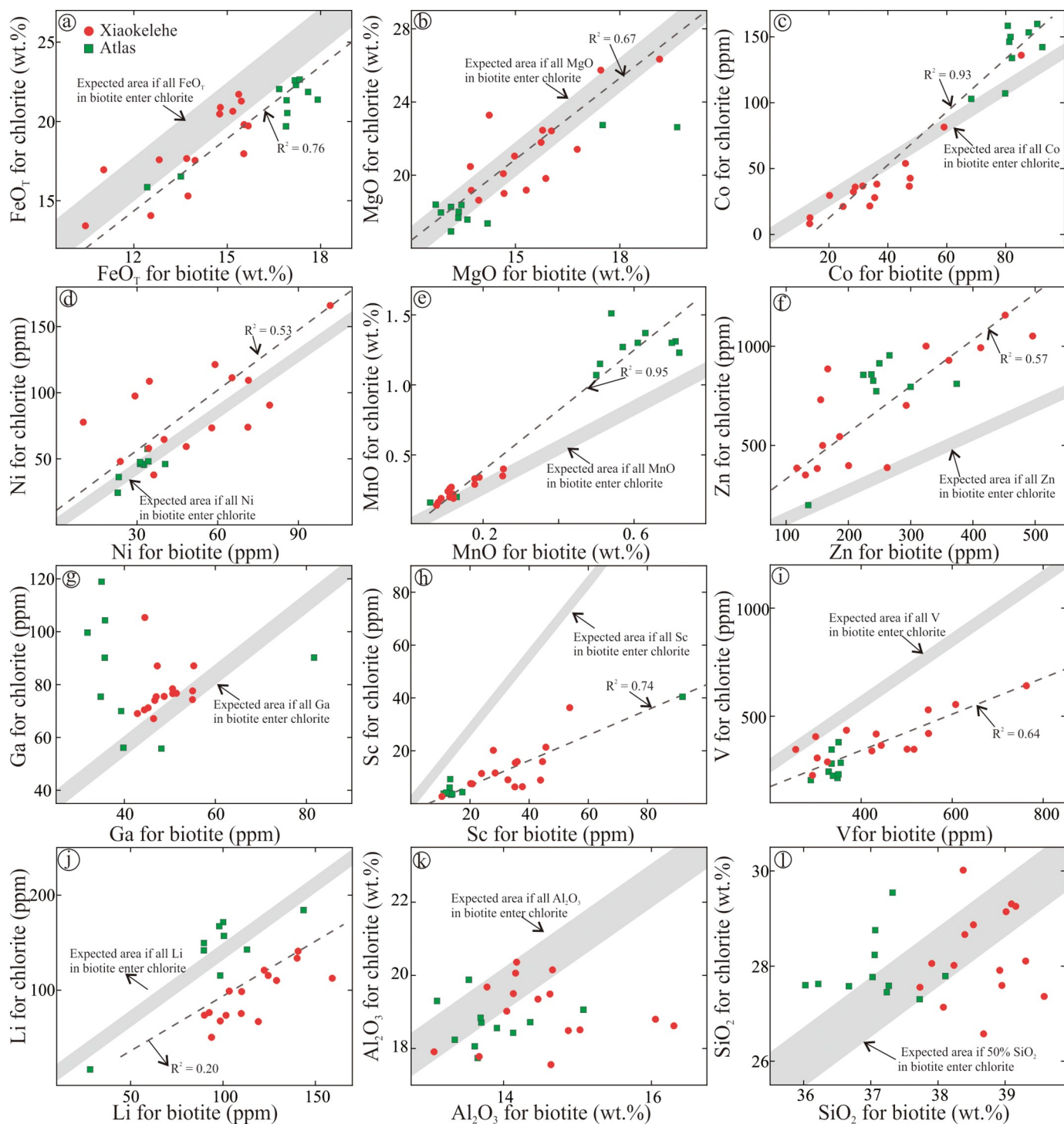


Fig. 5. FeO_T (a), MgO (b), Co (c), Ni (d), MnO (e), Zn (f), Ga (g), Sc (h), V (i), Li (j), Al_2O_3 (k), and SiO_2 (l) for biotite and chlorite of Xiaokelehe and Atlas analyses from individual crystals.

agree with previous studies, which have also shown that Al and Ti can be mobile in metamorphic fluids (Tropper and Manning, 2005; Audétat and Keppler, 2005; Gao et al., 2007; Antignano and Manning, 2008).

Based on transmission and scanning electron microscopy analysis, biotite is partially altered to chlorite mainly through the mechanism of layer-by-layer replacement (Jiang and Peacor, 1994), which results in metasomatic textures similar to those seen in Atlas and Xiaokelehe B-chlorite (Fig. 2b and d). Two chloritization mechanisms are proposed for the layer-by-layer replacement. The first involves $1\text{Bt} \rightarrow 1\text{Chl}$, meaning that one biotite layer is transformed into one chlorite layer,

forming an octahedral layer (Fe–O, Mg–O, and Al–O octahedrons) into the interlayer region between two TOT (tetrahedron-octahedron-tetrahedron) biotite layers, and characterized by a large inflow of metallic ions (Al^{3+} , Fe^{2+} , and Mg^{2+}) from the hydrothermal fluid into octahedral sheet in chlorite. The second is $2\text{Bt} \rightarrow 1\text{Chl}$, meaning that two biotite layers become one chlorite layer, forming a brucite-like layer by removal of the tetrahedral sheets (Si–O and Al–O tetrahedron) of one TOT biotite layer, and involving little or no inflow of metallic ion (s) from the hydrothermal fluid (Eggleton and Banfield, 1985; Yuguchi et al., 2015). In both mechanisms none of the K in the potassium sheet

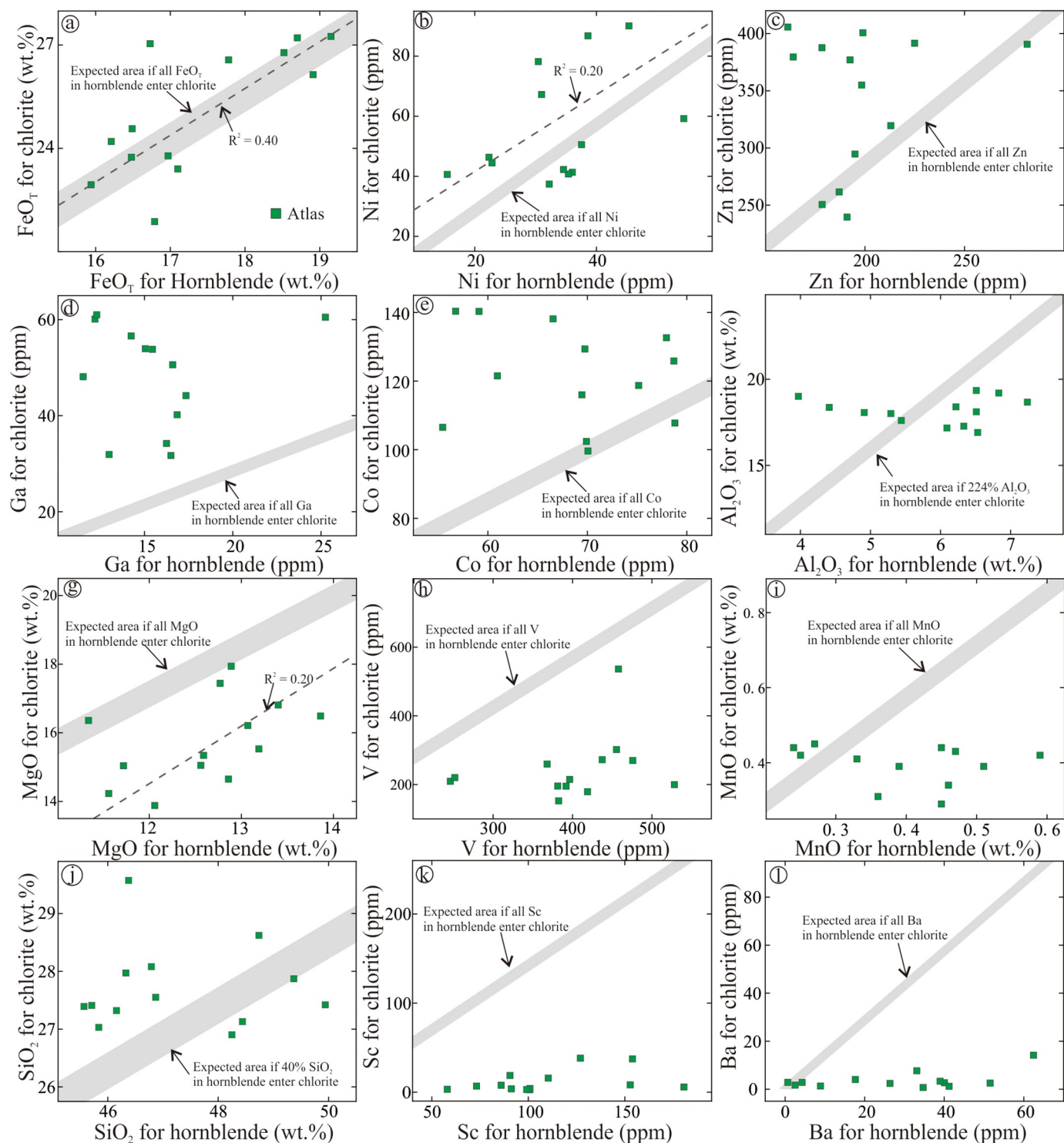


Fig. 6. FeO_T (a), Ni (b), Zn (c), Ga (d), Co (e), Al_2O_3 (f), MgO (g), V (h), MnO (i), SiO_2 (j), Sc (k), and Ba (l) for hornblende and chlorite of Atlas analyses from individual crystals.

of the biotite would not enter chlorite. The FeO_T and MgO contents of Xiaokelehe and Atlas B-chlorite are positively correlated with that of biotite, and close to or in the range of calculated compositions (Fig. 5a, b), indicating these elements were mostly retained in chlorite during chloritization, with no or very little inflow of these elements from the hydrothermal fluid. Moreover, Al_2O_3 and SiO_2 in Xiaokelehe and Atlas B-chlorite all deviate from the calculated values (Fig. 5k, l), indicating that at least some of these elements do not enter chlorite, which is consistent with the $2\text{Bt} \rightarrow 1\text{Chl}$ mechanism. Therefore, we suggest that

the mechanism $2\text{Bt} \rightarrow 1\text{Chl}$ is the main mechanism for Xiaokelehe and Atlas biotite chloritization (Fig. 8a).

By comparing the calculated and analytical values of elements in chlorite with those in hornblende, the FeO_T (avg. 100%) of Atlas H-chlorite were mostly retained in the chlorite; part of Ni (avg. 18%), Zn (avg. 19%), Co (avg. 19%), Al_2O_3 (avg. 55%), and Ga (avg. 56%) in the Atlas H-chlorite were derived from hydrothermal fluids; and part of MgO (avg. 12%), MnO (avg. 21%), V (avg. 56%), and SiO_2 (avg. 59%) in Atlas hornblende entered hydrothermal fluids, epidote or titanite,

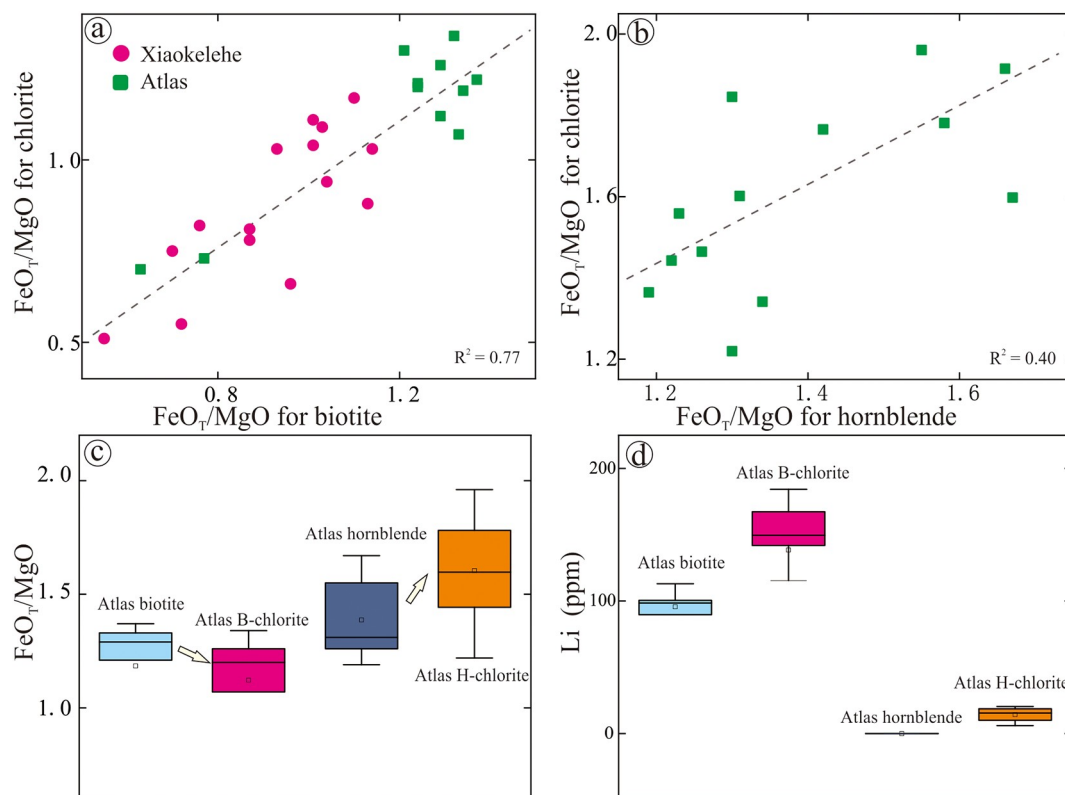


Fig. 7. FeO_T/MgO for biotite and chlorite of Xiaokelehe and Atlas (a), and hornblende and chlorite of Atlas (b) from individual crystals; Geochemical comparison of FeO_T/MgO (c), Li (d), between Atlas hornblende, biotite and chlorite.

Table 1

The average proportions of elements in biotite entering chlorite.

K	Nb	Ba	Rb	Ti	Cl	Na	Sn	Cu	Sc	Sr
0	0	0	0	2%	4%	7%	10%	18%	27%	42%

SiO_2	V	Li	Ni	FeO_T	Al_2O_3	MgO	Co^a	Ga^a	MnO^a	Zn^a
53%	63%	73%	92%	92%	95%	97%	122%	130%	142%	210%

^a Indicating part of elements in Xiaokelehe and Atlas B-chlorite is from hydrothermal fluid. Co (avg. 18%), Ga (avg. 23%), MnO (avg. 29%), and Zn (avg. 52%) in Xiaokelehe and Atlas B-chlorite are from hydrothermal fluid.

Table 2

The average proportions of elements in hornblende entering chlorite.

Ca	Zr	Nb	Sn	Cl	REE	Y	Na	Ti	Sr	K	Sc
0	0	0	0	0	0	1%	3%	4%	5%	5%	7%

Ba	SiO_2	V	MnO	MgO	FeO_T	Ni^a	Zn^a	Co^a	Al_2O_3^a	Ga^a
8%	41%	44%	79%	88%	100%	122%	124%	124%	224%	226%

^a Indicating part of elements in Atlas H-chlorite is from hydrothermal fluid. Ni (avg. 18%), Zn (avg. 19%), Co (avg. 19%), Al_2O_3 (avg. 55%), and Ga (avg. 56%) in Atlas H-chlorite are from hydrothermal fluid.

rather than chlorite, during Atlas hornblende chloritization (Fig. 6). Atlas H-chlorite contain ~ 20 ppm Li and ~ 200 ppm Cu, whereas Atlas hornblende contains no Li and minor Cu. Therefore, Cu and Li of Atlas H-chlorite could be from hydrothermal fluid, which may be derived from magma differentiation of the Atlas quartz diorite porphyry. In addition, the Ca, Zr, Nb, Sn, Cl, REE, Y, Na, Ti, Sr, K, Sc and Ba contents of Atlas H-chlorite are orders of magnitude lower than in the Atlas

hornblende (Appendixes I and II), suggesting that hornblende chloritization results in Ca (almost 100%), Zr (almost 100%), Nb (almost 100%), Sn (almost 100%), Cl (almost 100%), REE (almost 100%), Y (avg. 99%), Na (avg. 97%), Ti (avg. 96%), Sr (avg. 95%), K (avg. 95%), Sc (avg. 93%) and Ba (avg. 92%) in hornblende enter hydrothermal fluid, titanite or epidote, rather than chlorite. Epidote could accommodate Ca, Sr, Y, Sn, and REE (Xiao et al., 2018). Similar to biotite, elements behavior in the hornblende chloritization processes could be also controlled by solubility of elements in biotite and chlorite.

Hornblende is a double chain silicate, while chlorite is a phyllosilicate mineral. Such difference means that chlorite is unlikely to inherit hornblende structure during hornblende chloritization. Textual relationship of chlorite with hornblende (Fig. 2e) indicates that hydrothermal fluid may have replaced and dissolved hornblende, and then forming chlorite through precipitation processes in situ. Iron in hornblende is mostly retained in chlorite, indicating chlorite inherited Fe–O octahedrons of hornblende during chloritization. Therefore, chlorite formed during hornblende chloritization probably through processes of dissolution and precipitation (Fig. 8b).

5.2. Influence of precursor minerals on chlorite compositions

Previous studies have investigated the influence of wall rock on the chemical compositions of chlorite, and found that wall rocks mainly affect Fe/Mg ratio of chlorite (Kranidiotis and MacLean, 1987; Shikazono and Kawahata, 1987; De Caritat et al., 1993). Deng et al. (2019) and Zhang et al. (2019) have presented whole rock major and trace element analyses for the Atlas quartz diorite porphyry and Xiaokelehe granodiorite porphyry, which both show limited ranges. Hence, geochemical variations of chlorite in this study may have little relation with host rock compositions. According to studies on the relationship between trace elements of chlorite and its formation temperature (T), Xiao et al. (2018) has found that Li, Sr, Mn, and Zn contents show

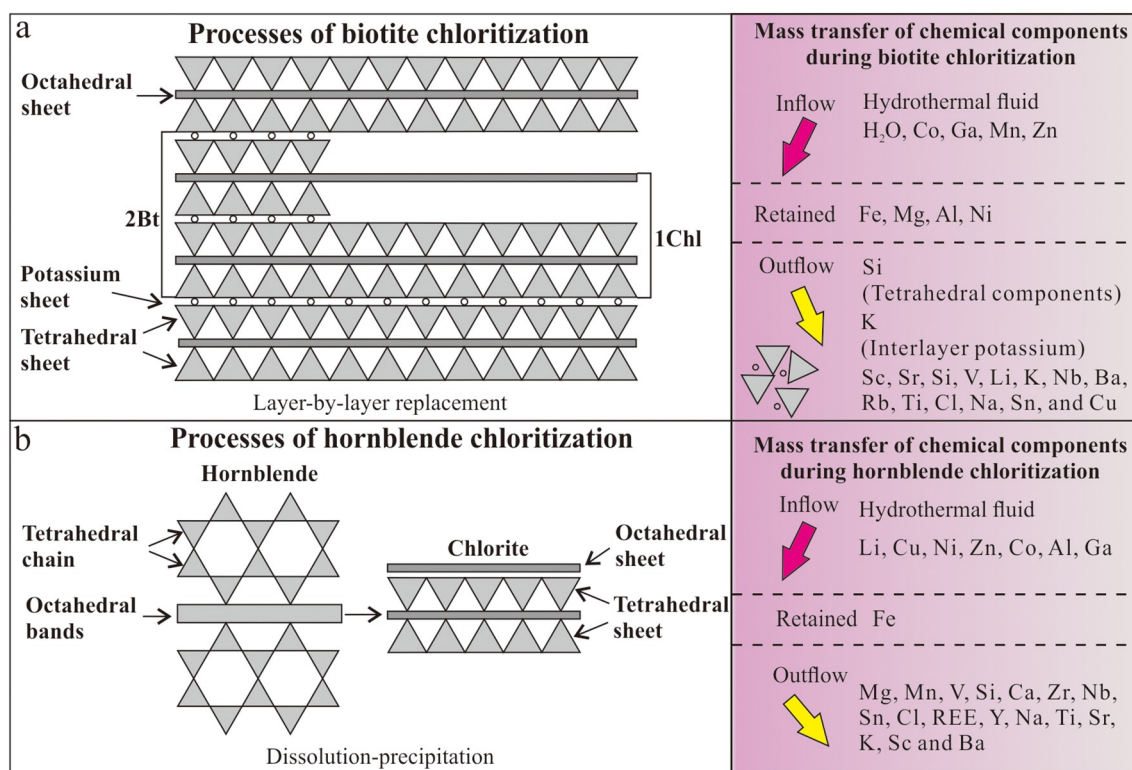


Fig. 8. Schematic figure showing development of crystal geometry (modified after Yuguchi et al., 2015) and mass transfer of chemical components in the biotite (a) and hornblende (b) chloritization processes.

negative correlations with T, while Sc, V, Ti, Ga, K, Ca, Co, Ni, Rb, Cs and Ba contents are positively associated with T, indicating that these elements of chlorite are controlled by its formation temperature.

Based on their geochemical behavior during chloritization, elements of chlorite can be divided into two groups. Group I including Fe, Ga, and SiO₂ has similar behavior in both biotite and hornblende chloritization. Iron in biotite and hornblende are mostly (> 90%) retained in chlorite during chloritization. The similar behavior of Fe in biotite and hornblende chloritization may be related to similar Fe contents in biotite and hornblende. The low contents of Ga in biotite and hornblende and the high ability for chlorite to enrich Ga (Négre et al., 2018) together result the contribution of Ga from hydrothermal fluid during chloritization (> 23%). At least some SiO₂ (> 47%) in hornblende and biotite does not enter chlorite during alteration, which should be related to lower solubility of SiO₂ in chlorite than that of biotite and hornblende. Group II includes MgO, Co, Ni, Mn, Zn, V, Sc and Al which show different behavior during biotite and hornblende chloritization: MgO, Co and Ni in Xiaokelehe and Atlas B-chlorite comes almost entirely (> 90%) from biotite, while part of MgO (12%) in hornblende enter hydrothermal fluid and part of the Co and Ni in Atlas H-chlorite (> 18%) is from the hydrothermal fluid; part of Mn (29%) in Xiaokelehe and Atlas B-chlorite comes from hydrothermal fluid, whereas part of Mn (21%) in hornblende does not enter chlorite during chloritization; the Zn, V and Sc contents of Xiaokelehe and Atlas B-chlorite show positive correlation with those of biotite, while there are no correlation between Atlas H-chlorite and hornblende; part of Al in Atlas H-chlorite comes from the hydrothermal fluid, which may be related to feldspar sericitization (Fig. 2e), during which Al could be released (Parneix et al., 1985; Morad et al., 2009), while Al in biotite mostly (> 90%) enter Xiaokelehe and Atlas B-chlorite. These different elements behavior in the biotite and hornblende chloritization processes could be mostly related to different contents and crystal structure of hornblende and biotite.

The FeO_T and MgO contents, and FeO_T/MgO ratios of chlorite are correlated with that of biotite, with correlation coefficient of 0.76, 0.67,

and 0.77, respectively (Figs. 5a, b, 7a). Moreover, those of Atlas H-chlorite also show weakly positive correlations with that of hornblende (Figs. 6a, b, 7b), indicating these elements and ratios are strongly influenced by associated precursor minerals. FeO_T/MgO ratios of Atlas B-chlorite are higher than those of Atlas B-chlorite (Fig. 7c), consistent with higher FeO_T/MgO ratios in Atlas hornblende than biotite. Fe and Mg in biotite mostly remain in chlorite during biotite chloritization, whereas Fe in hornblende remains in chlorite but some Mg (about 20%, Fig. 6g) does not enter chlorite, which results in FeO_T/MgO ratios of Atlas B-chlorite being close to or below that of Atlas biotite, whereas FeO_T/MgO ratios of Atlas H-chlorite are higher than that of Atlas hornblende. Hence, it can be speculated that the influence of wall rock on Fe/Mg ratios of chlorite proposed in previous studies (Kranidiotis and MacLean, 1987; Shikazono and Kawahata, 1987) is probably due to the different type and amount of precursor minerals in wall rock, although the Fe/Mg ratio variation of chlorite could also depend on changes in water/rock ratio, fO₂, fS₂, and pH as well as composition of the hydrothermal fluid (Kranidiotis and MacLean, 1987). Under high fS₂ conditions, the existence of pyrite results in Fe-poor chlorite, and Mg-rich chlorite appears to form under slightly oxidizing and low pH conditions (Inoue, 1995). Moreover, the influence of the FeO/Fe₂O₃ ratio is very important for understanding Fe³⁺ behavior in the biotite and hornblende chloritization. However, measuring the Fe³⁺ content at the microscale is challenging and could be only confirmed using X-ray absorption near edge-structure (XANES) which is not available in this study.

The MnO, Zn, Li, Sc, V, Co, and Ni contents of chlorite are strongly correlated with that of biotite in Xiaokelehe and Atlas (Fig. 5). Therefore, the MnO, Zn, Li, Sc, V, Co, and Ni contents of chlorite are not only influenced by its formation temperature according to the study of Xiao et al. (2018), but also by that of precursor minerals (e.g., biotite). In addition, the MnO and Zn contents of Atlas B-chlorite are markedly higher than that of Atlas H-chlorite, although Atlas B-chlorite and H-chlorite formed in the same porphyry system. The Li contents of Atlas

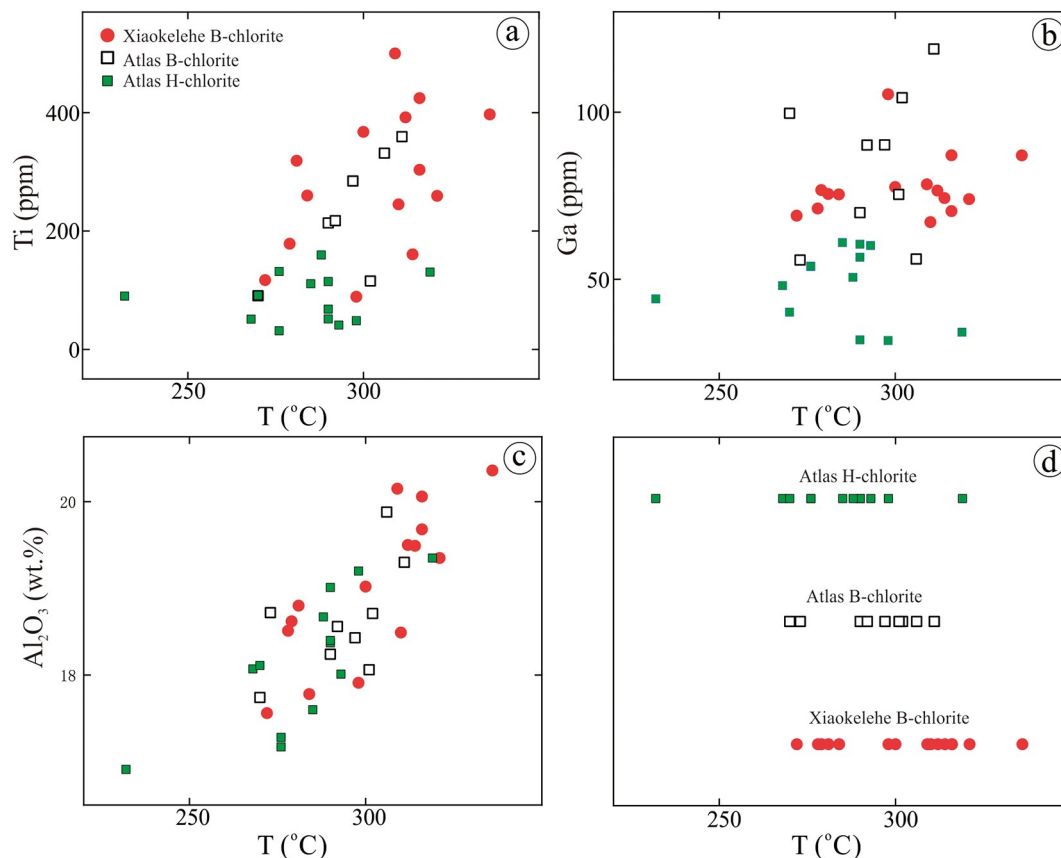


Fig. 9. Element concentrations in chlorite of this study vs. chlorite formation temperatures. (a) Ti; (b) Ga; (c) Al_2O_3 , and (d) chloritization temperatures according to chlorite thermometer of Cathelineau (1988).

H-chlorite (< 20 ppm) are lower than those of Atlas B-chlorite (most > 100 ppm), which may be related to that Atlas hornblende does not contain Li, while Atlas biotite have moderate contents of Li (about 100 ppm, Fig. 7d). Atlas and Xiaokelehe biotite contain low contents of Cu, and Atlas hornblende have moderate contents of Cu, for comparison, the Cu contents of B-chlorite are close or below the detection limits of LA-ICP-MS, while H-chlorite contains high contents of Cu (most > 100 ppm, Appendix II). Therefore, the MnO, Zn, Li and Cu contents of chlorite are also affected by the nature of the precursor minerals.

The Al_2O_3 and Ga contents of chlorite are higher than that of biotite and hornblende, and the Ti contents of chlorite are markedly lower (Appendixes I and II). The Ti, Ga, and Al_2O_3 , contents of chlorite show no obviously correlations with that of biotite and hornblende (Figs. 5 and 6, Appendix III), but have positive correlation with formation temperature of chlorite (Fig. 9), indicating these elements are not controlled by precursor minerals, but probably by formation temperature of chlorite (Xiao et al., 2018). The same behavior of Ga and Al may be related to that Ga shares a strong chemical affinity with Al (De Argollo and Schilling, 1978). The K, Ba, Sr and Rb contents of chlorite (close to or below the detection limits of LA-ICP-MS) are much lower than that of biotite and hornblende, and show no obvious correlations (Appendix III), also indicating they are not controlled by precursor minerals.

5.3. Implications for chlorite geothermometers and geochemical vectors for hydrothermal centers

Since the 1980s, chlorite compositions have been considered as a good proxy for estimating formation temperatures (Cathelineau and Nieva, 1985; Kranidiotis and MacLean, 1987). Based on the significant

positive correlation between the tetrahedral aluminum (Al^{IV}) and the measured temperature of chlorite in the active geothermal system, Cathelineau (1988) established an empirical equation: $T (^{\circ}\text{C}) = 321.98 * \text{Al}^{\text{IV}} - 61.92$. Considering the positive correlation between Al^{IV} and $\text{Fe}/\text{Fe} + \text{Mg}$, several tentative corrections have been introduced in the empirical equations (Kranidiotis and MacLean, 1987; Jowett, 1991; El-Sharkawy, 2000). Furthermore, a linear correlation has been found between the (001) basal spacing of chlorite and its formation temperature (Battaglia, 1999). In addition, thermodynamic and semi-thermodynamic calculation of formation temperatures for chlorites have also been proposed by previous studies (Vidal et al., 2001; Inoue et al., 2010; Lanari et al., 2014; Bourdelle and Cathelineau, 2015), which are valid on the premise of the chlorite + quartz equilibrium.

Thermodynamic and semi-thermodynamic thermometers are not used for chlorites in this study as they do not all coexist with quartz. Precursor minerals have obvious influence on the Mn and Li contents of chlorite, thus the empirical equations proposed by Battaglia (1999) could also be flawed based on this study. $\text{Fe}/(\text{Fe} + \text{Mg})$ ratios of chlorite are controlled by the compositions of precursor minerals in wall rock during hydrothermal alteration, and Bourdelle et al. (2013) also found that $\text{Fe}/(\text{Fe} + \text{Mg})$ ratios of chlorite in Gulf Coast sandstones have no correlation with its formation temperature. Therefore, the $\text{Fe}/(\text{Fe} + \text{Mg})$ correction on the thermometers for chlorite from alteration process may be inappropriate. Although Bourdelle et al. (2013) found empirical chlorite thermometers of Cathelineau (1988) could over-estimate the temperature of chlorite, the Al^{IV} values of chlorite still show obviously positive correlation with the temperature of chlorite. Consequently, we calculated the formation temperatures of Xiaokelehe B-chlorite, and Atlas B-chlorite and H-chlorite, using the chlorite thermometer of Cathelineau (1988) without the $\text{Fe}/(\text{Fe} + \text{Mg})$ corrections,

which yielded temperatures of 272–321 °C (average of 299 °C) for Xiaokelehe B-chlorite; 270–311 °C (average of 295 °C) for Atlas B-chlorite; and 232–319 °C (average of 283 °C) for Atlas H-chlorite. The temperature ranges for all studied chlorites are broadly the same (Fig. 9d), which is consistent with similar Al contents of Xiaokelehe B-chlorite, and Atlas B-chlorite and H-chlorite.

Trace element compositions of alteration minerals (e.g., chlorite, epidote) as mineral geochemical vectoring tools in exploration for porphyry deposits, have been widely studied in the recent years (Cooke et al., 2014; Jago et al., 2014; Wilkinson et al., 2015). At Batu Hijau, Wilkinson et al. (2015) found that K, Li, Mg, Ca, Sr, Ba, Ti, V, Mn, Co, Ni, Zn and Pb, display systematic spatial variations from the porphyry hydrothermal center: Ti, V and Mg concentrations decrease exponentially with increasing distance, whereas K, Li, Ca, Sr, Ba, Mn, Co, Ni, Zn and Pb concentrations increase. Such chlorite spatial variations extend to at least 4.5 km from the porphyry orebody, giving a much larger footprint than whole rock geochemical anomalies (≤ 1.5 km). In this study, we found that Fe, Mg, Co, and Ni in biotite, and Fe and Ni in hornblende are mostly retained in chlorite, which suggests that these elements are likely derived by progressive leaching from biotite or hornblende during chloritization, rather than from mineralization fluid of porphyry system. Hence, using these elements of chlorite from biotite and hornblende chloritization as geochemical vectors may not be appropriate. The MnO, Zn, Li and Cu contents of chlorite from biotite and hornblende chloritization are obviously different, though formed in the same porphyry system. Hence, we should be very cautious when use these elements as geochemical vectors, although Mn, Zn, and Li display systematic spatial variations from the porphyry hydrothermal center (Wilkinson et al., 2015). The Ti, Al, and Ga contents of chlorite are not controlled by precursor minerals, but by formation temperature of chlorite, so we can use these elements of chlorite to map out the thermal structure of porphyry system which is related to individual mineralized porphyry intrusion, which can help to identify the centers of hydrothermal systems.

6. Conclusions

This study has placed important constraints on elemental behavior during chlorite alteration in porphyry copper systems through a combined EMPA-LA-ICPMS study of two large porphyry Cu deposits, Atlas (Philippines) and Xiaokelehe (NE China). We observed that Fe and Mg are mostly retained in chlorite, whereas some of the Mn, Zn, and Ga in chlorite comes from hydrothermal fluid, and Sc, V, Li, Sr, Na, Ti, Cl, Cu, Rb, Nb, Sn, and Ba in biotite mostly do not enter chlorite during biotite chloritization; Fe mostly retained in chlorite, part of Li, Cu, Al, Zn, Ga, Ni, and Co in chlorite come from hydrothermal fluid, and Mn, Mg, Si, V, Sc, Na, K, Ca, Ti, Sr, Y, Zr, Nb, Sn, Ba, REE, and Cl in hornblende mostly enter hydrothermal fluid, titanite or epidote, rather than chlorite during hornblende chloritization. The MgO, Fe_T, MnO, Zn, Li, Sc, V, Co and Ni concentrations, and Fe_T/MgO ratio of chlorite from biotite and hornblende chloritization are markedly different, although formed in the same porphyry system. These results provide good instructions for geothermometers and geochemical vectors of chlorite for hydrothermal deposits.

Supplementary data to this article can be found online at <https://doi.org/10.1016/j.chemgeo.2020.119604>.

Declaration of Competing Interest

The authors declare that they have no known competing financial interests or personal relationships that could have appeared to influence the work reported in this paper.

Acknowledgements

This study was funded by the Chinese National Science Fund for Chinese National Science Foundation (41702068, U1603244), National Science Fund for Distinguished Young Scholars (41725009) and Chinese Academy of Sciences Strategic Pilot Science and Technology Special (XDB18000000). We thank Dr. P. Hollings for his assistance with the English in this paper. Constructive comments by Afifé El Korh, two anonymous reviewers, and editor Hailiang Dong helped to improve the manuscript.

References

- Antignano, A., Manning, C.E., 2008. Rutile solubility in H₂O, H₂O–SiO₂, and H₂O–NaAlSi₃O₈ fluids at 0.7–2.0 GPa and 700–1000 °C: implications for mobility of nominally insoluble elements. *Chem. Geol.* 255, 283–293.
- Audétat, A., Keppler, H., 2005. Solubility of rutile in subduction zone fluids, as determined by experiments in the hydrothermal diamond anvil cell. *Earth Planet. Sci. Lett.* 232, 393–402.
- Battaglia, S., 1999. Applying X-Ray geothermometer diffraction to a chlorite. *Clay Clay Miner.* 47, 54–63.
- Beaufort, D., Rigault, C., Billon, S., Billault, V., Inoue, A., Inoue, S., Patrier, P., 2015. Chlorite and chloritization processes through mixed-layer mineral series in low-temperature geological systems—a review. *Clay Miner.* 50, 497–523.
- Bernard, P.C., Van Grieken, R.E., Eisma, D., 1986. Classification of estuarine particles using automated electron microprobe analysis and multivariate techniques. *Environ. Sci. Technol.* 20, 467–473.
- Bourdelle, F., Cathelineau, M., 2015. Low-temperature chlorite geothermometry: a graphical representation based on a T–R²⁺–Si diagram. *Eur. J. Mineral.* 27, 617–626.
- Bourdelle, F., Parra, T., Chopin, C., Beyssac, O., 2013. A new chlorite geothermometer for diagenetic to low-grade metamorphic conditions. *Contrib. Mineral. Petrol.* 165, 723–735.
- Brzozowski, M.J., Samson, I.M., Gagnon, J.E., Linnen, R.L., Good, D.J., Ames, D.E., Flemming, R., 2018. Controls on the chemistry of minerals in late-stage veins and implications for exploration vectoring tools for mineral deposits: an example from the Marathon Cu–Pd deposit, Ontario, Canada. *J. Geochem. Explor.* 190, 109–129.
- Cathelineau, M., 1988. Cation Site Occupancy in Chlorites and Illites as a Function of Temperature. *Clay Miner.* 23, 471–485.
- Cathelineau, M., Nieva, D., 1985. A chlorite solid solution geothermometer the Los Azufres (Mexico) geothermal system. *Contrib. Mineral. Petrol.* 91, 235–244.
- Cooke, D.R., Baker, M., Hollings, P., Sweet, G., Chang, Z.S., Danyushevsky, L., Gilbert, S., Zhou, T.F., White, N.C., Gemmill, J.B., 2014. New advances in detecting the distal geochemical footprints of porphyry systems—epidote mineral chemistry as a tool for vectoring and fertility assessments. *Econ. Geol. Spec. Publ.* 18, 127–152.
- De Argollo, R., Schilling, J.G., 1978. Ge-Si and Ga-Al fractionation in Hawaiian volcanic rocks. *Geochim. Cosmochim. Acta* 42, 623–630.
- De Caritat, P., Hutcheon, I., Walshe, J.L., 1993. Chlorite geothermometry: a review. *Clay Clay Miner.* 41.
- Deng, C.Z., Sun, D.Y., Han, J.S., Li, G.H., Feng, Y.Z., Xiao, B., Li, R.C., Shi, H.L., Xu, G.Z., Yang, D.G., 2019. Ages and petrogenesis of the Late Mesozoic igneous rocks associated with the Xiaokele porphyry Cu–Mo deposit, NE China and their geodynamic implications. *Ore Geol. Rev.* 107, 417–433.
- Dora, M.L., Randive, K.R., 2015. Chloritisation along the Thanewasna shear zone, Western Bastar Craton, Central India: its genetic linkage to Cu–Au mineralisation. *Ore Geol. Rev.* 70, 151–172.
- Eggleton, R.A., Banfield, J.F., 1985. The alteration of granitic biotite to chlorite. *Am. Mineral.* 70, 902–910.
- El-Sharkawy, M.F., 2000. Talc mineralization of ultramafic affinity in the Eastern Desert of Egypt. *Mineral. Deposita* 35, 346–363.
- Feng, Y.Z., Xiao, B., Li, R.C., Deng, C.Z., Han, J.S., Wu, C., Li, G.H., Shi, H.L., Lai, C.K., 2019. Alteration mapping with short wavelength infrared (SWIR) spectroscopy on Xiaokelehe porphyry Cu–Mo deposit in the Great Xing’an Range, NE China: metallogenic and exploration implications. *Ore Geol. Rev.* 112, 103062.
- Foley, S.F., Barth, M.G., Jenner, G.A., 2000. Rutile/melt partition coefficients for trace elements and an assessment of the influence of rutile on the trace element characteristics of subduction zone magmas. *Geochim. Cosmochim. Acta* 64, 933–938.
- Fu, Y., Sun, X.M., Hollings, P., Li, D.F., Yang, T.J., 2018. Geochronology and trace element geochemistry of titanite in the Machangqing Cu–Mo-dominated polymetallic deposit, Yunnan Province, southwest China. *J. Asian Earth Sci.* 158, 398–414.
- Gao, J., John, T., Klemm, R., Xiong, X.M., 2007. Mobilization of Ti–Nb–Ta during subduction: evidence from rutile-bearing dehydration segregations and veins hosted in eclogite, Tianshan, NW China. *Geochim. Cosmochim. Acta* 71, 4974–4996.
- Hart, L., Wilkinson, J., Armstrong, R., Araujo, D., 2016. Element mobility during propylitic alteration in porphyry ore systems: a case study of the Oyu Tolgoi deposits, Mongolia. *Appl. Earth Sci.* 125, 84.
- Inoue, A., 1995. Formation of Clay Minerals in Hydrothermal Environments. *Origin and Mineralogy of Clays*. Springer.
- Inoue, A., Kurokawa, K., Hatta, T., 2010. Application of chlorite geothermometry to hydrothermal alteration in Toyoha geothermal system, southwestern Hokkaido, Japan. *Resour. Geol.* 60, 52–70.
- Jago, C.P., Tosdal, R.M., Cooke, D.R., Harris, A.C., 2014. Vertical and lateral variation of mineralogy and chemistry in the Early Jurassic Mt. Milligan alkalic porphyry Au–Cu

- deposit, British Columbia, Canada. *Econ. Geol.* 109, 1005–1033.
- Jiang, W.T., Peacor, D.R., 1994. Formation of corrensite, chlorite and chlorite-mica stacks by replacement of detrital biotite in low-grade pelitic rocks. *J. Metamorph. Geol.* 12, 867–884.
- Jowett, E., 1991. Fitting iron and magnesium into the hydrothermal chlorite geothermometer. In: GAC/MAC/SEG Joint Annual Meeting, Toronto, May 27–29, 1991, Program with Abstracts.
- Kranidiotis, P., MacLean, W.H., 1987. Systematics of chlorite alteration at the Phelps Dodge massive sulfide deposit, Matagami, Quebec. *Econ. Geol.* 82, 1898–1911.
- Krivovichev, S.V., Armbruster, T., Organova, N.I., Burns, P.C., Seredkin, M.V., Chukanov, N.V., 2004. Incorporation of sodium into the chlorite structure: the crystal structure of glagolevite, $\text{Na}(\text{Mg,Al})_6[\text{Si}_3\text{AlO}_{10}](\text{OH},\text{O})_8$. *Am. Mineral.* 89, 1138–1141.
- Lanari, P., Wagner, T., Vidal, O., 2014. A thermodynamic model for di-trioctahedral chlorite from experimental and natural data in the system $\text{MgO-FeO-Al}_2\text{O}_3\text{-SiO}_2\text{-H}_2\text{O}$: applications to P-T sections and geothermometry. *Contrib. Mineral. Petrol.* 167, 968.
- Morad, S., El-Ghali, M.A.K., Caja, M.A., Al-Ramadan, K., Mansurbeg, H., 2009. Hydrothermal alteration of magmatic titanite: evidence from Proterozoic granitic rocks, Southeastern Sweden. *Can. Mineral.* 47, 801–811.
- Négre, P., Ladenberger, A., Reimann, C., Birke, M., Sadeghi, M., 2018. Distribution of Rb, Ga and Cs in agricultural land soils at European continental scale (GEMAS): Implications for weathering conditions and provenance. *Chem. Geol.* 479, 188–203.
- Parneix, J.C., Beaufort, D., Dudoignon, P., Meunier, A., 1985. Biotite chloritization process in hydrothermally altered granites. *Chem. Geol.* 51, 89–101.
- Parry, W.T., Downey, L.M., 1982. Geochemistry of hydrothermal chlorite replacing igneous biotite. *Clay Clay Miner.* 30, 81–90.
- Shang, Y.G., 2017. Study on the Geological Characteristics and Metallogenic Prognosis of Xiaokele and 972 Highland Gold Polymetallic Deposit in Daxinganling, Heilongjiang Province. Master Degree Thesis. Jilin University.
- Shikazono, N., Kawahata, H., 1987. Compositional differences in chlorite from hydrothermally altered rocks and hydrothermal ore deposits. *Can. Mineral.* 25, 465–474.
- Sillitoe, R.H., 2010. Porphyry copper systems. *Econ. Geol.* 105, 3–41.
- Sillitoe, R.H., Gappe, I.M., 1984. Philippine porphyry copper deposits: geologic setting and characteristics. In: CCOP-ESCAP Technical Publication. vol. 14. pp. 89.
- Singer, D.A., Berger, V.I., Moring, B.C., 2008. Porphyry copper deposits of the world—database and grade and tonnage models. In: 2008: U.S. Geological Survey Open-File Report 2008-1155, accessed June 1, 2011, at. <http://pubs.usgs.gov/of/2008/1155/>.
- Tropper, P., Manning, C.E., 2005. Very low solubility of rutile in H_2O at high pressure and temperature, and its implications for Ti mobility in subduction zones. *Am. Mineral.* 90, 502–505.
- Vidal, O., Parra, T., Trotet, F., 2001. A thermodynamic model for Fe-Mg aluminous chlorite using data from phase equilibrium experiments and natural pelitic assemblages in the 100° to 600°c, 1 to 25 kb range. *Am. J. Sci.* 301, 557–592.
- Walker, J.R., 1993. Chlorite polytype geothermometry. *Clay Clay Miner.* 41, 260.
- Wang, Z.Q., Chen, B., Yan, X., Li, S.W., 2018. Characteristics of hydrothermal chlorite from the Niujuan Ag-Au-Pb-Zn deposit in the north margin of NCC and implications for exploration tools for ore deposits. *Ore Geol. Rev.* 101, 398–412.
- Wiewióra, A., Weiss, Z., 1990. Crystallochemical classifications of phyllosilicates based on the unified system of projection of chemical composition: II. The Chlorite Group. *Clay Miner.* 25, 83–92.
- Wilkinson, J.J., Chang, Z.S., Cooke, D.R., Baker, M.J., Wilkinson, C.C., Inglis, S., Chen, H.Y., Bruce Gemmel, J., 2015. The chlorite proximator: a new tool for detecting porphyry ore deposits. *J. Geochem. Explor.* 152, 10–26.
- Xiao, B., Chen, H.Y., Hollings, P., Wang, Y.F., Yang, J.T., Wang, F.Y., 2018. Element transport and enrichment during propylitic alteration in Paleozoic porphyry Cu mineralization systems: Insights from chlorite chemistry. *Ore Geol. Rev.* 102, 437–448.
- Yavuz, F., Kumral, M., Karakaya, N., Karakaya, M.Ç., Yıldırım, D.K., 2015. A Windows program for chlorite calculation and classification. *Comput. Geosci.* 81, 101–113.
- Yuguchi, T., Sasao, E., Ishibashi, M., Nishiyama, T., 2015. Hydrothermal chloritization processes from biotite in the Toki granite, Central Japan: temporal variations of the compositions of hydrothermal fluids associated with chloritization. *Am. Mineral.* 100, 1134–1152.
- Zhang, Y., Tian, J., Hollings, P., Gong, L., Albuero, I., Berador, A.E., Francisco, D.G., Li, J., Chen, H.Y., 2019. Mesozoic porphyry Cu–Au mineralization and associated adakite-like magmatism in the Philippines: insights from the giant Atlas deposit. *Mineral. Deposita*. <https://doi.org/10.1007/s00126-019-00907-2>.
- Zhong, R.C., Li, W.B., Chen, Y.J., Huo, H.L., 2012. Ore-forming conditions and genesis of the Huoqeqi Cu–Pb–Zn–Fe deposit in the northern margin of the North China Craton: evidence from ore petrologic characteristics. *Ore Geol. Rev.* 44, 107–120.